An elastically tethered viscous load imposes a regular gait on the motion of myosin-V. Simulation of the effect of transient force relaxation on a stochastic process

Maria J. Schilstra[1],[†] **and Stephen R. Martin**[2]

[1]*Biocomputation Research Group, STRI, University of Hertfordshire, College Lane, Hatfield AL10 9AB, UK*
[2]*Physical Biochemistry, National Institute for Medical Research, The Ridgeway, Mill Hill, London NW7 1AA, UK*

Myosin-V is a processive molecular motor that moves membrane vesicles along actin tracks. In the simple model for motor and cargo motion investigated here, an elastic connection between motor and cargo transiently absorbs the abrupt mechanical transitions of the motor, and allows smooth relaxation of the cargo to a new position. We use a stochastic description to model motor stepping, with kinetics that depends on the instantaneous force exerted on the motor through the elastic connection. Tether relaxation is modelled as a continuous process, in which the rate is determined by the viscous drag of the cargo and the stiffness profile of the connection. Quantitative combined stochastic–continuous simulation of the dynamics of this system shows that bulky loads can impose a highly regular gait on the motor. If the characteristics of the elastic connection are similar to those of the myosin-II coiled-coil domain, the myosin-V motor, tether and cargo form a true escapement, in which the motor only escapes from its current position after one or more force thresholds have been crossed. Multiple thresholds limit the variation in tether length to values below that of the total step size.

Keywords: myosin-V; modelling; force-dependent kinetics; non-Markov process; stochastic; hybrid simulation

1. INTRODUCTION

Myosin-V is a two-headed processive molecular motor that moves along actin filaments to transport a variety of cargo to its destination (Titus 1997; Reck-Peterson *et al.* 2000; Vale 2003). Myosin-V has been found associated with melanosomes, synaptic vesicles, and other vesicular organelles, which range from 0.05 to over 1 µm in diameter (Evans *et al.* 1998; Tabb *et al.* 1998).

Like the other members of the extended myosin family, the heavy chain of myosin-V has an *N*-terminal motor domain, followed by a neck and a tail domain. Its lever arm extends to 24 nm when stabilized by six calmodulin molecules, and enables the myosin-V dimer to take 36 nm steps along the actin filament. A distinctive feature of myosin-V, at least of the variants found in higher eukaryotes, is the relatively large region—some 500 amino acid residues (Espreafico *et al.* 1992)—that is predicted to form an α-helical coiled-coil. Only the heavy chain of myosin II has a longer coiled-coil region with over 1000 amino acid residues (Maita *et al.* 1991). It is believed that the coiled-coil regions in myosins allow dimerization into two-headed structures (Sellers 2000), and that they function as spacers between the motors and their cargo.

A consensus mechanism for myosin-V motility has emerged from a number of single molecule and solution kinetics studies (Vale 2003 and references therein). In short: in the so-called waiting state, the myosin-V heads, both associated with ADP, bind simultaneously to two actin subunits that are separated by approximately 36 nm, the actin pseudo-repeat. Upon the release of ADP from the trailing head—the head furthest away from the plus-end of the actin filament—the nucleotide binding site is free to bind ATP. ATP binding causes the interaction between the trailing head and the actin filament to weaken, and the trailing head dissociates. After the trailing head has become detached, the arm with the trailing head swings past the leading head, finds a new actin subunit to bind to at about 72 nm from its previous position, and becomes the new leading head. The newly bound ATP is hydrolysed to ADP and inorganic phosphate (Pi)

[†]Author for correspondence (m.j.1.schilstra@herts.ac.uk).

during this process, but the phosphate ion can only escape from the nucleotide pocket when the new leading head is bound to the actin. Pi release returns myosin-V to its waiting state, translocated by 36 nm with respect to its previous position.

Two steps in the mechanism outlined above are slow compared to the others. In the absence of any external pulling or pushing forces, ADP release from the trailing head and ATP binding to the empty nucleotide pocket are estimated to occur with rate constants of the order of $10\,\mathrm{s}^{-1}$ and $1\,\mu\mathrm{M}^{-1}\,\mathrm{s}^{-1}$, respectively (De La Cruz *et al.* 1999). Dissociation of ADP from the leading head is probably much slower. If the kinetics of ADP and ATP binding were the same in the trailing and leading head, the coordination of the events in the two heads would be lost, and the motor would not be processive. It is believed that differences in tension between the heads are responsible for the differences in nucleotide binding kinetics. This tension is generated when, following the 'power stroke' (probably Pi release), the leading head is prevented—owing to its connection with the tightly bound trailing head—from adopting a conformation in which its lever arm points in the direction of the plus-end of the actin filament.

Evidence for tension-dependent kinetics has been provided by investigations of the effect of an externally applied force on myosin-V motility (Mehta *et al.* 1999; Rief *et al.* 2000; Veigel *et al.* 2001, 2005; Clemen *et al.* 2005). Kolomeisky & Fisher (2003) demonstrated that the observations reported by Mehta *et al.* (1999) and Rief *et al.* (2000) could be quantitatively described by a two-state periodic sequential kinetic model. They derived an analytical expression for the dependence of the mean dwell time on the ATP concentration and on the external force applied parallel to the motor track, and used it to estimate the dependence of the transition rates on the force. They found that the best fit forward transition rate constants were in excellent agreement with previously observed values (De La Cruz *et al.* 1999; Trybus *et al.* 1999), and that an external force increases the backward stepping rates, but barely affects the kinetics of the forward transitions.

In vitro observations on myosin-V stepping kinetics, including those used in the parameter optimization procedure mentioned above, are often made using a force clamp, in which a constant external force on the motor is maintained through an electronic feedback mechanism. *In vivo*, however, the force on the motor is unlikely to be constant. Bulky loads, such as the membrane vesicles that are myosin-V's cargo, resist being pulled through the cytosol, and generate a drag force that increases with their size and velocity. The 'staircase plots' of distance travelled against time, typical for myosin-V and other molecular motors, suggest that motor translocation itself occurs rapidly, even under loads that approach the stall force. If the cargo were connected to the motor through a very stiff connection, the motor would have to generate a force large enough, and for a sufficiently long time, to make the cargo follow its movement immediately: dragging a 100 nm diameter vesicle through a medium with a viscosity of $100\,\mathrm{Pa\,s}^{-1}$ (Bausch *et al.* 1999, see §2) over 10 nm in 10 ms would require a sustained force of 100 pN. A more flexible, elastic connection could absorb the immediate impact of an abrupt forward motion, and would allow the cargo to relax more gradually toward its new position, thereby reducing the instantaneous pull on the motor. Because of the probability that the motor takes another step is dependent on the force it experiences, the rate at which the cargo relaxes toward its new equilibrium position will affect the stepping behaviour of the motor.

To investigate the effect of cargo size and tether elasticity on the putative stepping characteristics of myosin-V, we have used the two-state model of Kolomeisky & Fisher (2003), coupled to a continuous spring relaxation process, to perform a simulation of myosin-V stepping. The transition probabilities depend on the instantaneous force, which depends on the residual force and on the time that has elapsed since the previous step. The dependence of the transition rates on the stepping history makes this a non-Markov process. Here, we describe an adaptation of the algorithm known as Gillespie's direct method to perform an exact stochastic simulation of chemical reactions whose kinetics are coupled to a continuous process. We show that a cargo with realistic dimensions, connected to the motor via a fully elastic tether with plausible characteristics, not only slows down the motor, but also makes it step in a uniform, periodic fashion.

2. METHODS

2.1. *Model for myosin-V and cargo motion*

The model for myosin-V and cargo motion, shown in figure 1, describes a processive motor that steps stochastically along a fixed track, and is connected via an elastic spring to a cargo. The lifetimes of the motor states depend on the force that the motor is subjected to. The position of the motor along the axis parallel to the track, as well as the external force on the motor (the frictional force generated by the moving cargo), are measured at point C, the motor's centre of internal forces. Each transition between motor states is associated with a translocation of C along the track, and can be forward as well as backward. A state transition causes an instantaneous change in the length of the spring equal to the distance travelled by C, and, since an extended spring has a tendency to return to its equilibrium length, a change in the force on the motor. The position of the motor is fixed between transition events, but the cargo is allowed to move. The motion of the cargo under the restoring force of the spring generates a drag force proportional to its current velocity, and opposite to its direction of motion.

2.2. *Kinetic model for motor motion*

The simulations discussed in this paper are based on Kolomeisky & Fisher's (2003) two-state kinetic model, including the equations that quantitatively describe this model, and the parameter values that form the best fit to the observed dynamics of myosin-V processivity. The model has states S0 and S1, and reversible transitions between S0 and S1 and S1 and S0. Each
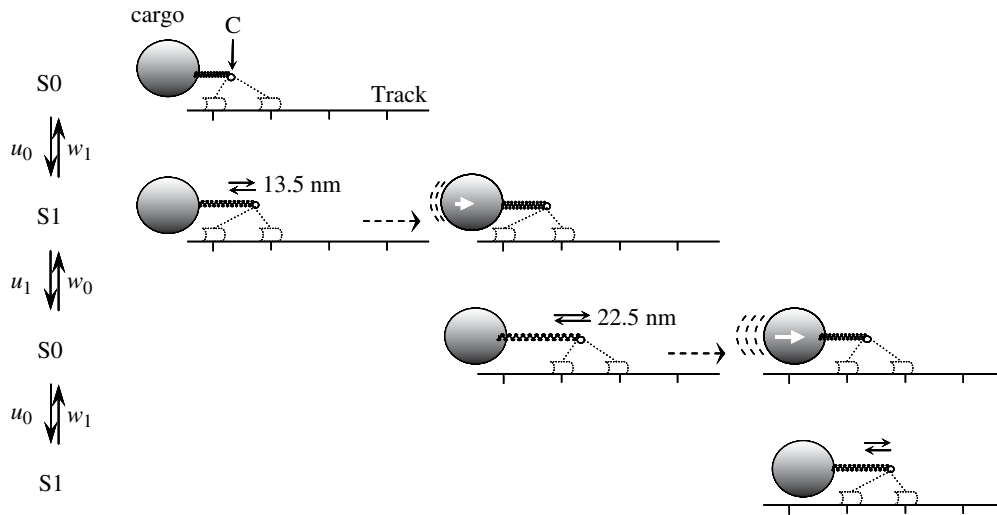
Figure 1. Cartoon representation of the model used in the simulations. At the centre of force C (small circle), a cargo (large circle) is connected via a spring (zigzag) to the two-legged processive molecular motor myosin-V. Myosin-V is bound to an actin track via its two motor heads, one leading and one trailing (light and dark grey semi-transparent polygons and dotted lines). The direction of forward motion is from left to right, so that the leftmost motor head is the trailing head, and the rightmost head is the leading one. The motor states (S0 and S1) and the symbols for the transition rates (u_0, w_1, u_1, w_0) are indicated on the left-hand side. During a sub-step the centre of force moves instantaneously over 13.5 or 22.5 nm. After completing of the S0 to S1 step, the trailing head becomes the leading head and *vice versa*. The cargo position is fixed during the instantaneous movements of the centre of force (through motor transitions), so that, as a result, the spring extension changes. In the finite intervals between motor transitions, the position of the centre of force is fixed, and the spring relaxes in a continuous way towards its equilibrium length, hindered by the drag of the cargo. The motor is entirely free to make the next sub-step before the spring has reached its equilibrium length. Note, that the placement of the heads relative to the centre of force in this picture is tentative, and used solely to explain the concept of the motor–spring–cargo model, rather than the stepping mechanics.

rate is dependent on the total external force on the motor, to an extent specified in each load distribution factor. Equations (2.1)–(2.4) express the rate of each step as a function of the rate constant at zero force, k, the ATP concentration, [ATP], the load distribution factor, θ and the external force, F. The subscripts 0 or 1 indicate the state before the transition; the superscripts $+$ and $-$ denote forward and backward steps. D is the total distance that the motor moves upon one complete catalytic cycle (36 nm), k_B is Boltzmann's constant, and T the absolute temperature (293 K).

$$u_0 = k_0^+[\text{ATP}]\exp\left(-\theta_0^+ \frac{FD}{k_B T}\right), \qquad (2.1)$$

$$w_0 = k_0^-[\text{ATP}]\exp\left(\theta_0^- \frac{FD}{k_B T}\right), \qquad (2.2)$$

$$u_1 = k_1^+\exp\left(-\theta_1^+ \frac{FD}{k_B T}\right), \qquad (2.3)$$

$$w_1 = k_1^-\exp\left(\theta_1^- \frac{FD}{k_B T}\right). \qquad (2.4)$$

The (best-fit) parameter values that we used in the simulations are $0.7\times10^6\,\text{M}^{-1}\,\text{s}^{-1}$ and $12\,\text{s}^{-1}$ for the forward rate constants k_0^+ and k_1^+; $5\,\text{M}^{-1}\,\text{s}^{-1}$ and $6\times10^{-6}\,\text{s}^{-1}$ for the reverse rate constants k_0^- and k_1^-; and -0.01, 0.58, 0.045 and 0.385 for θ_0^+, θ_0^-, θ_1^+ and θ_1^-, respectively. Because the sum of the load distribution factors equals 1, $u_0 u_1/w_0 w_1 = (k_0^+ k_1^+/k_0^- k_1^-)\exp(-FD/k_B T)$. With the above parameter values, the stall force (where reverse stepping cancels forward stepping, and $u_0 u_1/w_0 w_1 = 1$) is 2.96 pN.

The expression for the mean forward dwell time, τ_+, in this system is $\tau_+ = (u_0 + u_1 + w_0 + w_1)/(u_0 u_1 + w_0 w_1)$. If the fraction of reverse steps is negligible (which, under these conditions, is the case for $F < 2.5$ pN) the overall velocity of the motor is calculated as $V = D\tau_+$ (equations and data from Kolomeisky & Fisher 2003). The system thresholds (see §3) are calculated from the force at which the probabilities of forward and reverse stepping from a particular state are equal, by solving $u_i/w_i = 1$ for F ($F_{eq} = (k_B T/D)\ln(k_i^+/k_i^-)/(\theta_i^+ + \theta_i^-)$).

The sums of the load distribution factors, $\theta_{01} = \theta_0^+ + \theta_1^-$ and $\theta_{10} = \theta_1^+ + \theta_0^-$, represent the fraction of the total free energy that is associated with the individual reversible sub-steps S0–S1 and S1–S0 under constant load. Thus, the S0–S1 step takes care of 38% of the total work ($-0.01 + 0.385$), which corresponds to a 13.5 nm translocation of the centre of force, whereas the remaining 62% of the work or translocation over 22.5 nm, is done during the S1–S0 transition. Similar sized sub-steps were observed in a later study by Uemura *et al.* (2004). The forward S0–S1 transition is dependent on the ATP concentration, and its best-fit value is in good agreement with the ATP association rate constant observed in independent measurements, whereas the best-fit value of the forward S1–S0 step is close to the ADP release rate measured in other studies (see §1).

2.3. Damped spring model for flexibly connected cargo

The tether that connects the cargo to point C on the motor is modelled as a fully elastic spring. All motor state transitions occur instantaneously, and during a transition

point C moves the full distance associated with the transition, whereas the cargo stays where it was. The result is an instantaneous change in the extension of the spring, and hence in the force exerted on the motor.

The relationship between the extension of the elastic tether between the motor and the cargo and the restoring force is almost certainly highly nonlinear. In their assessment of the elastic properties of the dimeric coiled-coil domain of the myosin-II heavy chain, Schwaiger *et al.* (2002) have found that this structure can extend by to up to 2.5 times its original length in a truly elastic manner. The extension is biphasic: under relatively low-pulling force (up to 25 pN), its length increases from 150 to 270 nm, and in the second phase it eventually extends by another 150 nm. The second phase starts abruptly when the extension is about 120 nm and probably includes a massive structural transition that occurs under a pulling force of 25–30 pN. Most of the extension (some 80%) in the first phase occurs upon increasing the force from 0 to 5 pN, whereas an additional 20 pN is required to bring about a further 20 nm increase in length. The second phase has a similar profile.

If the elastic properties of the myosin-V tether are similar to those of the myosin-II coiled-coil, it is possible to create an elasticity profile for the latter by applying the interpolation formula for the relation between force and extension in the worm-like chain (WLC) model (Bustamante *et al.* 1994; Rief *et al.* 1998; Schwaiger *et al.* 2002). Since the second phase in the extension profile of the myosin-II coiled-coil is observed at forces greater than 25 pN, we assume that the force–extension curve of the myosin-V coiled-coil can be described using the persistence length, L_P, for the low-force phase (25 nm) only. As the coiled-coil region in the myosin-II heavy chain is 1100 amino acid residues, and its contour length 150 nm, we assume that the contour length, L_C, of the myosin-V coiled-coil, which has 510 residues, is 70 nm. In this study, we have approximated the interpolation formula for the WLC model by a polynomial of the form

$$F = ax + (bx)^{\mathrm{P}}. \qquad (2.5)$$

Here, F is the spring's restoring force at extension x and a, b and p are phenomenological constants. The WLC interpolation curve for $L_C = 70$ and $L_p = 25$ nm (shown in figure 2), is approximated by the above polynomial with $p = 10$, $a = 0.005$ pN nm^{-1} and $b = 0.018$ (pN nm^{-1})$^{0.1}$. When $p = 1$, the expression for F reduces to Hooke's law and the spring stiffness, $\kappa = \mathrm{d}F/\mathrm{d}x$, is constant and equal to $a + b$. For higher order dependences, the spring's stiffness increases with increasing extension as $\kappa(x) = a + pb^P x^{P-1}$. The main reason for using the polynomial approximation rather than the WLC interpolation curve is that in our simulations the spring must be allowed (in principle) to jump to an extension greater than L_C, where the WLC interpolation curve is no longer valid (it has an asymptote at $x = L_C$). Another reason is that the equation of motion for $F = ax + (bx)^P$ has a relatively simple analytical solution (see below), facilitating the simulation procedure, and the analysis of the results.
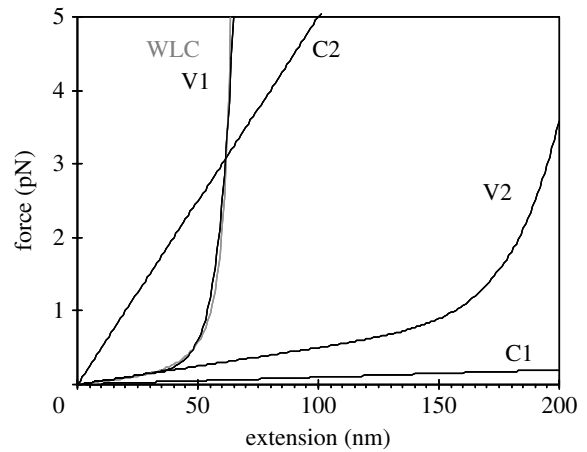

Figure 2. Force–extension profiles ($F = ax + (bx)^p$) for springs with various characteristics. Values for a, b and p: C1: 0, 0.001, 1; C2: 0, 0.05, 1; V1: 0.005, 0.018, 10; V2: 0.005, 0.0055, 10. WLC (grey curve): force–extension profile according to the worm-like chain model with parameters L_C, 70 nm; L_P, 25 nm (see text; analogous to those for myosin-II).

The frictional forces F_{fr} on the moving cargo are proportional to the cargo's velocity: $F_{\mathrm{fr}} = -\beta \mathrm{d}x/\mathrm{d}t$, where β is the frictional constant of the cargo. This proportionality is justified because Reynold's number is very much smaller than 1 at realistic cargo velocities (Happel & Brenner 1983). Between transitions, the position of the motor is fixed, but the cargo, which is not restrained, will move under the spring's restoring force. However, this movement is hindered by the frictional forces (the effect of inertia is negligible under these conditions). The expressions for the extension x at time t for $p = 1$ (Hooke's Law) and $p > 1$ are given in equations (2.6a) and (2.6b), respectively.

$$x(t) = x_0 \exp\left(-\frac{\kappa}{\beta} t\right), \qquad (2.6a)$$

$$x(t) = x_0 \left(\left(1 + \frac{b^p}{a} x_0^{p-1}\right) \exp\left((p-1)\frac{a}{\beta} t\right) \right.$$
$$\left. - \frac{b^p}{a} x_0^{p-1} \right)^{1/(1-p)}. \qquad (2.6b)$$

Here, x_0 is the extension at $t = 0$, the moment immediately after the transition, and is the sum of the instantaneous change in the spring extension, x_{step}, and the residual extension just before the transition, $x_{\mathrm{res}} : x_0 = x_{\mathrm{step}} + x_{\mathrm{res}}$.

2.4. Coupling motor and cargo motion

During a simulation, the motor transition probabilities are calculated from the instantaneous force on the motor, F, and must be constantly re-evaluated because F will vary significantly as the motor to load distance changes. Just before a motor state transition, the residual force on the motor, F_{res}, is equal to $ax_{\mathrm{res}} + (bx_{\mathrm{res}})^P$, whereas immediately after the transition it is $F_0 = ax_0 + (bx_0)^P$. The restoring force at ant time t after a transition event is obtained by substituting the expression for $x(t)$ (equation (2.6a) or (2.6b)) into that for F (equation (2.5)). This value of F is used

to calculate the appropriate transition rates by substitution in equations (2.1)–(2.4). Note that the equilibrium 'constants' in this model (u_0/w_1 and u_1/w_0) are very different immediately before and after a transition, and change between successive transitions. Furthermore, the work done during a transition (F integrated over x from x_{res} to x_0) is variable, and depends on the spring extension just before the transition.

Coupled stochastic–continuous simulations were carried out using a variant of the algorithm known as Gillespie's direct method (Bortz *et al.* 1975; Gillespie 1977). In this variant, particle states and their associated physical constants are represented individually, and a random number is generated for each possible transition (as there is just one particle, only two transitions are possible at any one time). The probability p_i that the *i*th transition from a given current state will have occurred, changes with time as

$$\frac{\mathrm{d}p_i}{\mathrm{d}t} = \alpha_i(1 - p_i). \qquad (2.7)$$

Here, α_i is the transition rate variable, and is substituted with u_0, u_1, w_0 and w_1 (equations (2.1)–(2.4)) in the simulations. Time is measured from the point at which the system changed to its current state, t_0, where $p_i = 0$. The time that the next transition will take place, $t_{next,i}$ is selected by solving the above differential equation for t with a random number r_i ($0 \leq r_i < 1$) substituted for p_i. The process is repeated for all possible transitions from the current state, and the transition for which $t_{next,i}$ is smallest is the one that occurs. For time-invariant α_i, $t_{next,i} = -\ln(1 - r_i)/\alpha_i$. However, when the time dependence of u_0, u_1, w_0 and w_1 is taken into account, equation (2.7) does no longer have an analytical solution, and must be solved numerically.

We used a fourth order Runge–Kutta algorithm (Press *et al.* 1989) to perform the integration up to the time point, where $r_i = p_i$. The simulation program used to obtain the results described below was written specifically for the purpose of simulating the model presented here, but has a facility to read, build, edit and write other models with similar characteristics. The simulator and its source code are available on request from M.J.S.

3. RESULTS

3.1. Characteristics of assorted spring systems

We have simulated the behaviour of various motor–spring–cargo combinations: a combination in which the spring is very soft (system C1, $\kappa = 0.001$ pN nm^{-1}), and can extend indefinitely without a change in its stiffness, one in which the spring is much stiffer (system C2, $\kappa = 0.05$ pN nm^{-1}), but still constant, and finally a combination in which the spring stiffness increases as the spring extends (system V1). The characteristics of spring in V1 are closest to those of the coiled-coil domain of myosin-V, assuming that the coiled-coil domain of myosin-II is about twice as long as that of myosin-V, and the other relevant

characteristics (in particular the persistence length) of the coiled-coil domains in both myosins are similar. Systems C1 and C2 are hypothetical, and are used to illustrate particular concepts. Figure 2 shows the force–extension relationships ('profiles') for the three types of spring.

Figure 3 contains typical simulated trajectories for the above motor–spring–cargo combinations. In each of the simulations, the ATP concentration is a constant, saturating 2 mM, and identical motors drag identical, sizeable loads (for which $\beta = 10^{-4}$ kg s^{-1}—*in vivo* this could be vesicles with diameters of 50–100 nm, see §4), but the springs between the motor and the cargo have different characteristics. At the start of each simulation, the spring is fully relaxed, but as soon as the motor begins to move, the spring stretches, and exerts a restoring force on the motor. Table 1 (top three rows) summarizes the results of the simulations as the mean velocity (of motor and cargo at steady state), $\langle V \rangle$, the mean restoring force of the spring, $\langle F \rangle$ (averaged over time), the mean oscillatory period, $\langle \delta \rangle$ (see below) and its standard deviation, $\sigma(\delta)$, the mean extension of the spring, $\langle x \rangle$ and its standard deviation, $\sigma(x)$.

3.1.1. Constant restoring force. The top row of figure 3 shows the behaviour of system C1, in which the cargo is connected to the motor via a very soft spring whose stiffness is constant. In this system, the motor initially moves at a velocity approaching a theoretical maximum (430 nm s^{-1}, calculated from the expression for the mean forward dwell time, see §2), but gradually slows down after the cargo has started moving under the spring's increasing restoring force. After 15–20 s, a steady state is reached where motor and cargo move at the same average velocity, with the cargo following far behind the motor.

The top right-hand panel, a close-up of motor and cargo movement at steady state, shows that the motion of the cargo in this constant force system is very smooth, and is correlated only with the overall forward movement of the motor. The motor, on the other hand, moves much more erratically, combining forward steps with a significant number of backward ones, and displays widely varying dwell times (where the dwell time is the interval between two consecutive full steps), with a standard deviation of 97% of the mean. Multiple consecutive full backward steps are frequently observed. Close inspection of the motor trajectory reveals that the 22.5 nm sub-steps occur much more frequently than the 13.5 nm transitions, as many forward S1→S0 transitions are followed rapidly by a backward S1←S0 sub-step. The S0→S1 transition, in contrast, appears to be successful on most, if not all, occasions.

An important aspect of this hypothetical system is that, at steady state, the force on the motor is virtually constant (here 2.41 ± 0.01 pN, indicated in the figure), because each step only results in a relatively small increase or decrease in the extension of the spring, and a correspondingly small change in its restoring force. Since the force on the motor is constant, the behaviour of system C1 is very similar to the behaviour of motors
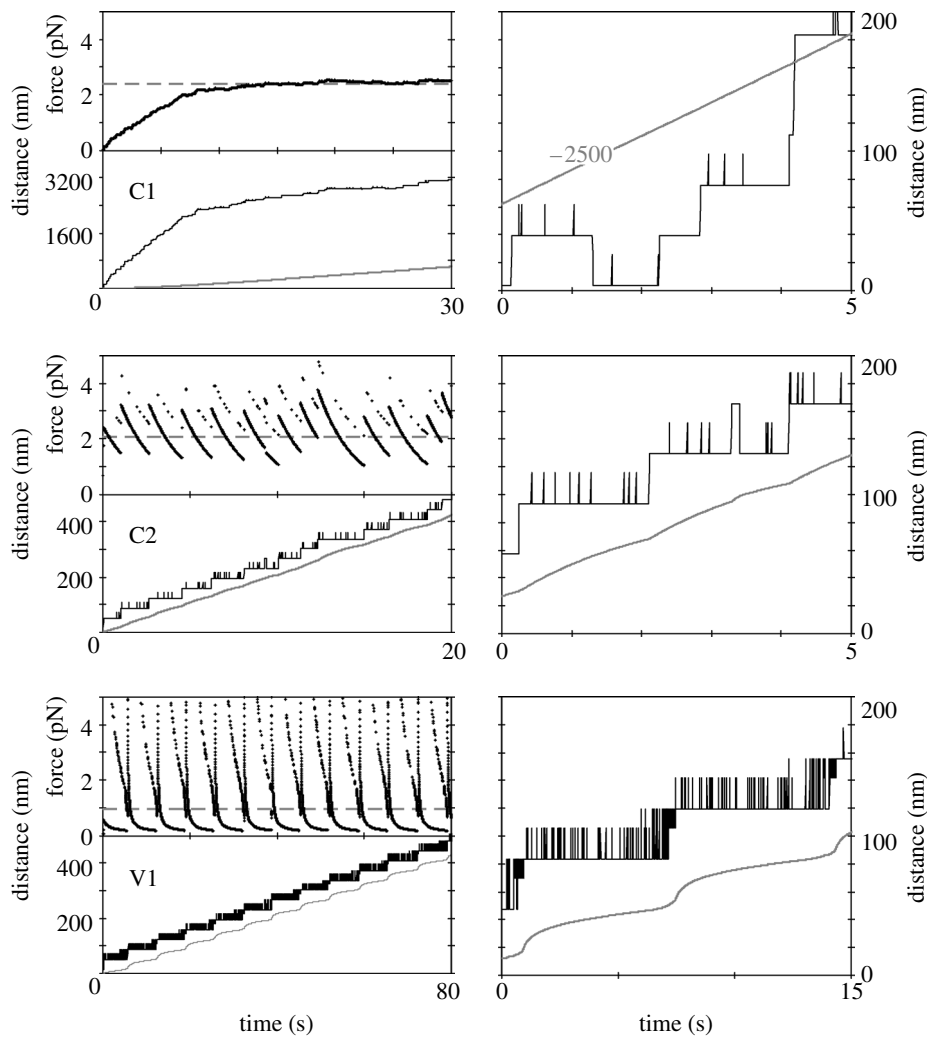
Figure 3. Characteristic behaviour during the initial 30 s of a simulation of a motor dragging a large cargo ($\beta = 10^{-4}\,\mathrm{kg\,s^{-1}}$) at saturating [ATP] (2 mM). Top: system C1 (spring stiffness coefficient $\kappa = 0.001\,\mathrm{pN\,nm^{-1}}$, constant for all extensions); middle: system C2 ($\kappa = 0.05\,\mathrm{pN\,nm^{-1}}$, constant); bottom: system V1 (κ varies; spring characteristics analogous to those for myosin-II). Left column, top panels: force trajectories; grey dashed horizontal line: average force on the motor. Bottom panels: motor (black) and cargo (grey) trajectories. Right column: close-up over 5 (C1 and C2) or 15 s (V1) of the simulated motor and cargo trajectories. Note that the position of the cargo in C1 has been offset by 2.5 μm.

in experimental set-ups in which the cargo is held in an optical trap, and where the force on the motor is kept constant by means of an electronic feedback system. By varying the value of the drag coefficient β in the simulations, a range of constant forces can be applied to the motor, and in the electronic supplementary material we show that the dependence of the average dwell time on the force on the motor in this system is indeed as observed *in vitro* by Rief *et al.* (2000), and follows the theoretical curve derived by Kolomeisky & Fisher (2003).

3.1.2. Variable restoring force—constant stiffness. The second row of figure 3 shows the motor, cargo and force trajectories for system C2, in which the spring's stiffness is still independent of the extension, but is now so large that each sub-step produces a significant change in force on the motor. System C2 has a much shorter transient period; the extension of the spring varies mostly between 20 and 60 nm, and never exceeds 100 nm. Both the steady-state velocity of motor and

cargo and the average force on the motor are about 80% of the values for system C1. The close-up shows that the relative frequency of the 22.5 nm S1↔S0 transitions has increased, and that each full forward step is now reflected to a certain extent in the movement of the cargo. Full backward steps are rare, and they usually happen shortly after a full forward step. The stepping of system C2 is more regular than that of system C1: the standard deviation of the dwell times is about 15%, and the motor never makes two (or more) consecutive full backward steps. Any 'premature' full forward step is followed relatively quickly by a full backward one, until a point is reached where the spring has relaxed sufficiently (see below), and a 'successful' forward step is made. In this system, and the ones discussed below, it is useful to define the oscillatory period, δ, as the interval between successful full forward steps. Thus, the definition of δ is different from the definition of the dwell time, τ, the interval between two full steps, be it forward or backward. The close-up of the motor trajectory of system C2 illustrates the difference: the

Table 1. Simulation results. (a, b, p: spring parameters; β: frictional constant of cargo; $\langle V \rangle$, $\langle F \rangle$, $\langle \delta \rangle$, $\langle x \rangle$: average steady-state velocity, force on the motor, oscillatory period and extension; $\sigma(\delta)$, $\sigma(x)$: standard deviation of δ and x; $X(\text{thr}_0)$, $X(\text{thr}_1)$: calculated extensions at the force thresholds of 2.3 and 3.8 pN.)

system	a (pN nm^{-1})	b (pN$^{0.1}$ nm^{-1})	p	β (10^{-4} kg s^{-1})	$\langle V \rangle$ (nm s^{-1})	$\langle F \rangle$ (pN)	$\langle \delta \rangle$ (nm)	$\sigma(\delta)$ (nm)	$\langle x \rangle$ (nm)	$\sigma(x)$ (nm)	$X(\text{thr}_0)$ (nm)	$X(\text{thr}_1)$ (nm)
C1	0	0.001	1	1.0	25	2.4	1.3	1.3	2494	37	2300	3800
C2	0	0.05	1	1.0	20	2.1	1.8	0.3	43	13	46	76
V1	0.005	0.018	10	1.0	5	0.9	6.7	0.3	55	11	60	63
$L_P = 50$	0.0025	0.018	10	1.0	4	0.7	9.3	0.4	54	12	60	63
$L_P = 12.5$	0.01	0.018	10	1.0	8	1.2	4.7	0.2	55	11	59	62
$L_C = 140$	0.005	0.009	10	1.0	14	1.4	2.7	0.2	107	11	117	125
$L_C = 35$	0.005	0.036	10	1.0	2	0.3	23.0	0.3	25	12	30	32
V2	0.005	0.0055	10	1.0	20	1.9	1.8	0.2	180	11	188	201
C1	0	0.001	1	1.3	20	2.6	1.6	1.5	2580	43	2300	3800
V1	0.005	0.018	10	0.27	20	0.8	1.8	0.1	54	11	60	63

dwell times, τ, are 1.9, 1.0, 0.2 and 0.8 s, whereas the intervals between the two successful steps, δ, are 1.9 and 2.0 s.

3.1.3. Variable restoring force—stiffness dependent on extension.

The bottom row of figure 3 contains the trajectory for a motor–spring–cargo combination in which the spring stiffness increases as the spring extends, and whose characteristics are (arguably) similar to those of the coiled-coil domain in myosin-V. The stepping in this system is characterized by a very large increase in the force on the motor immediately after a forward step (much greater than the stall force, but only briefly), followed by a short phase during which the force decreases rapidly, and a much longer second phase, during which the force changes much more slowly. The average force on the motor is less than 1 pN, because the system spends much of the time in the second, low-force regime. System V1 makes many forward steps that are almost immediately followed by a step in the opposite direction. Like system C2, the system oscillates between S1 and S0, for some time after a successful forward step, and at a later stage also makes full S1–S0–S1 transitions in both directions. In the last stage of the period between two successful forward steps, unlike system C2, the system oscillates with a very high frequency (up to 1000 s^{-1}) between S0 and S1, until the extension decreases below a certain threshold (see below), and no further backward S0←S1 transitions are made. At that point, the motor has completed another oscillatory period. The movement of the cargo is highly correlated with that of the motor: as the restoring force of the spring is large at the beginning of a step, the motor moves more quickly during the first phase, then slows down. However, when the motor starts trying to make the full S1–S0–S1 transition, the restoring force, and with it the velocity of the cargo, increases again, and reaches a maximum at the time that the step is complete. The average period between two successful forward steps is considerably longer in system V1 than in systems C1 and C2, and as a result motor and cargo move more slowly along the track. However, the variation

in the length of the period is significantly smaller: 4.5% of the mean for V1 versus 17% for C2 and 97% for C1.

3.2. Regularity and uniformity

Figure 3 indicates that motor–spring–cargo combinations in which the restoring force of the spring decreases significantly in the interval between two successful full forward steps move with much greater regularity than combinations in which the force is virtually constant. Since the forward rates (u_0 and u_1, equations (2.1) and (2.3)) are virtually independent of the force on the motor, forward stepping occurs more or less at the same frequency, regardless of the spring extension. However, 'overambitious' forward steps in the variable force systems (C2 and V1) will result in the force on the motor immediately becoming very high, and because of the associated increase in the propensity of the backward steps (w_0 and w_1, equations (2.2) and (2.4)), such steps will be aborted almost immediately (by a backward step). Only when the force has reduced enough will one forward sub-step be followed by another forward sub-step. Premature forward steps and their compensating backward steps tend to occur more often shortly before a successful forward step, and are usually followed relatively quickly by a new attempt to step forward.

3.2.1. Cargo size.

The rate at which the spring relaxes depends on the drag coefficient of the cargo, β, and together with the spring characteristics, β determines the regularity and uniformity of motor and cargo motion. Cargo with a small viscous drag moves faster than larger cargo that is subjected to the same force, so that a spring connecting the smaller cargo to the motor will relax more rapidly. If the spring is able to relax very quickly, the interval between successive full forward steps will no longer be determined by the time required for the cargo to move under the spring's restoring force, but by the intrinsic (probabilistic) forward and backward stepping rates of the motor at zero force. Likewise, in constant force systems such as system C1, a forward step may be followed rapidly by several further forward

steps, without a very large change in force on the motor. Although the ratio of reverse to forward (sub-)steps increases with increasing cargo size, the stepping behaviour is, again, probabilistic. As a result, the motion of the variable force systems is more uniform than that of the constant force system C1, and this effect becomes more pronounced as the load size increases (see the electronic supplementary material for a more complete comparison of the behaviour of systems C1 and C2 under increasing load).

3.2.2. Spring stiffness at low extension (persistence length). In system V1, where the spring's stiffness increases with its extension, stepping is, in general, even more regular than in system C2 (under load, the systems show a similar decrease in regularity for decreasing β). This is because, at large extensions, a small decrease in extension results in a relatively large decrease in the force on the motor. As a result, the intermediate region between the zone where the propensity of backward stepping is high, and the one in which backward stepping is unlikely, is narrow, and crossed rapidly. The duration of the interval δ between two successful full forward transitions is dependent on the rate at which the spring relaxes from its extension immediately after the successful jump, x_{start}, to the extension from where it can jump again ($x_{end} = x_{start} - 36$ nm). This rate is determined to a large extent by the stiffness at low extension: if the stiffness is very small before the extension has decreased to x_{end}, the cargo will move very slowly under the spring's associated small restoring force, and the interval between forward jumps will be long. The stiffness at low extension is determined mainly by the value of a (in our pheno-menological equation), whose value is (roughly) inver-sely proportional to the persistence length L_P in the WLC model. Table 1 shows that the oscillatory period, which is 6.7 s for system V1, becomes 4.7 and 9.3 s for values of a that are double and half of the value a in V1, respectively (and increases to 21 s when a is zero, not shown). In all of these cases, the average velocity and force on the motor change concomitantly, but the average spring extension remains roughly the same.

3.2.3. Spring length (contour length). The average spring extension is determined for a large part by b, whose value is related to the contour length L_C in the WLC model. If b is half the size of b in V1, which roughly corresponds to a doubling in L_C, the average extension changes from 55 to 107 nm, whereas the period δ decreases by a factor of 2.5. The length of the oscillatory period is about 40% of that in V1, whereas the average force on the motor is 1.5 times higher. If the spring is shorter ($b = 0.036$, corresponding with $L_C = 35$ nm), its average extension, 25 nm, is only two thirds of the step size (36 nm). The oscillatory period is significantly longer (23 s), whereas the average force on the motor is only 0.3 pN.

3.2.4. Regularity of systems moving at the same velocity. A change in the spring's stiffness profile or length is always accompanied by changes in both the length of the oscillatory period (and hence the overall velocity) and average force on the motor. The size of the cargo determines the velocity that can be achieved in a particular system: the only way of making a particular system go faster or slow down (in these simulations) is to decrease or increase its load. On the other hand, systems with seemingly different characteristics may actually progress at the same velocity under equal load conditions. We have investigated the effect of the spring profile on the regularity and uniformity of motion for combinations that move at the same velocity (20 nm s^{-1}) as system C2 when it carries a load for which $\beta = 10^{-4}$ kg s^{-1} (figure 3). The results are summarized in the bottom rows of table 1, and the variations in spring extension, as well as the deviations of the cargo from a path of uniform motion are shown in figure 4. The figure also contains plots of the simulated dwell time distributions (i.e. the intervals between two full steps, forward or backward).

Like system C2, system V2 (spring profile in figure 2, spring parameters correspond to contour and persist-ence lengths of 25 and 220 nm, respectively) moves at 20 nm s^{-1} while dragging a cargo of 10^{-4} kg s^{-1}. In both systems, each full backward step is followed by a forward step, and the oscillatory period is 1.8 s. The deviations of the cargo from a path of uniform motion have a high frequency component (0.55 s^{-1}), which reflects the individual steps, and also have lower frequency noise (deviations of ± 10 nm, 0.01 s^{-1}) due to slight variations in the overall velocity of the system. The variations in the spring extension are similar in both systems: the amplitude is almost equal; the variation in the length of the oscillatory period is somewhat larger in system C2 (15%) than in V2 (10%). This is reflected in the distribution of the dwell times, in which the second mode (around 1.8 s) represents full forward steps, and is slightly narrower for V2. The first mode (closest to 0) is caused by backward stepping of the motor, which in both systems is relatively infrequent, and occurs mostly towards the end of the oscillatory period. The main difference in the behaviour of these systems is the average extension of the spring: 43 nm in C2 and 180 nm in V2. The spring profiles (figure 2) reveal the reason for the difference and similarities in the behaviour of these two systems: in V2, the spring stiffness at extensions between 160 and 200 nm is approximately equal to that of the spring in C2.

The velocity of the very soft spring system C1 is 25 nm s^{-1} when $\beta = 10^{-4}$ kg s^{-1}, whereas system V1, in which the spring stiffness increases steeply at an extensions above 50 nm, has an average velocity of only 5 nm s^{-1}. System C1 requires a load of 1.3×10^{-4} kg s^{-1} to slow it down to 20 nm s^{-1}, and system V1 needs it load reduced to 0.27×10^{-4} kg s^{-1} to achieve the same velocity. Under these conditions, these two systems show very different behaviour. In both cases the low-frequency noise in the path of the cargo is less that in system C2 (deviations of ± 2 nm in C1 and ± 5 nm in V1), but individual motor steps are not at all reflected in the cargo motion in system C1, and very strongly that in system V1. System C1 exhibits large variations in spring extension, and its
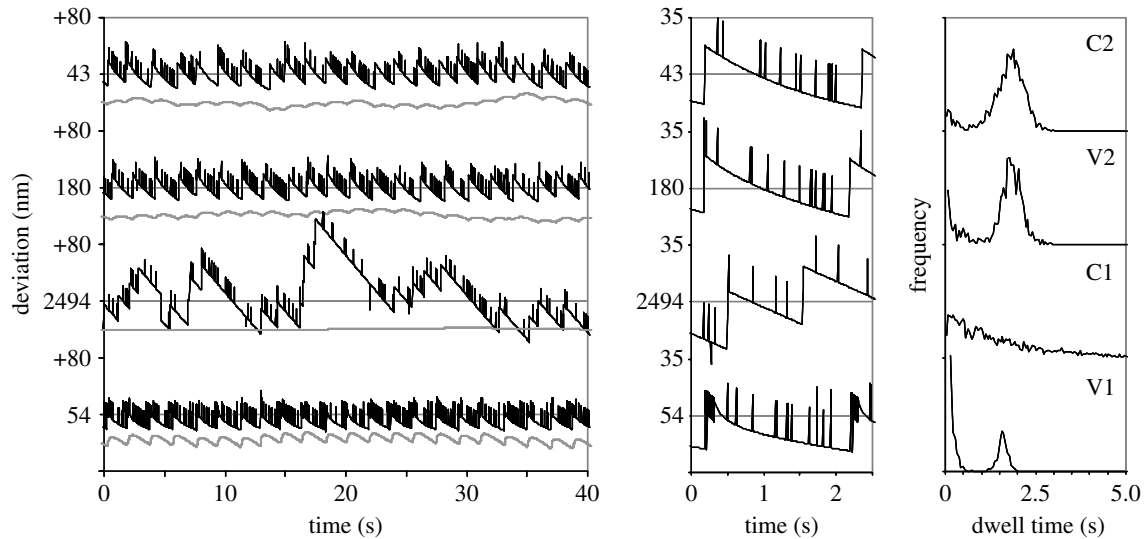
Figure 4. Behaviour of systems with different spring characteristics, all moving at an average velocity of 20 nm s^{-1}. Panels from top to bottom: C2, V2, C1, V1. Left panels: variation of the spring extension (black lines) and cargo position (grey lines) around their averages (whose values are indicated; the cargo positions have been offset by -40 nm). Middle panels: close-up of the spring extension trajectories over 2.5 s. c: distribution of the dwell times (interval between two full S1–S0–S1 transitions, including the 'unsuccessful' ones).

dwell times are widely distributed. The dwell time distribution has a single mode, and there is no distinction between forward and backward steps. Since both forward and backward steps occur at random intervals, there is no determined oscillatory period, and the values listed under $\langle\delta\rangle$ and $\sigma(\delta)$ in table 1 are the mean dwell time and its standard deviation. On the other hand, the variation is spring extension in system V1 is even smaller than in C1 and C2, and the length of the oscillatory period is well defined, with a standard deviation of 5%. Backward stepping occurs frequently, but only during the 0.2 s before a successful forward step. Therefore, the dwell time distribution has a prominent first mode, and the centre of the second mode is shifted to 1.6 s.

3.3. Sub-step frequency and thresholds

Close inspection of the trajectories in figures 3 and 4 reveals that the motor is in the S1 state for most of the time, and from there makes many short excursions to the S0 state, whose centre of force lies 22.5 nm further forward. Forward and backward stepping between S0 and S1 over the next 13.5 nm occurs infrequently in systems C1 and C2, but is very frequent in system V1. To understand this behaviour, it is necessary to consider the position of two thresholds in the model. When the motor is in the S0 state, and force is greater than 2.3 pN, it is more likely that it will step backward over 22.5 nm (S1←S0) than forward over 13.5 nm (S0→S1; see §2). When the motor is in the S1 state, and the force is greater than 3.8 pN, the probability that it will make a backward transition (S0←S1, -13.5 nm) is greater than the probability that it will go forward (S1→S0, $+22.5$ nm). In system C2 the force on the motor is 2.3 pN when the extension of the spring is 44 nm. If the system is in state S0, and the extension is smaller than 44 nm, the next sub-step is likely to be a

forward one, yielding a new spring extension of 58 nm, and a restoring force of 2.9 pN. The system is now in the S1 state, and the force is still much smaller than 3.8 pN. Therefore, the probability that the motor will step backward is very small, and the next sub-step is most likely to be a forward one over 22.5 nm (S1→S0), which increases the force on the motor by another 1.1 pN. If these forward steps have occurred in short succession, the spring's restoring force may be as large as 4 pN at this point in the cycle. The next successful forward sub-step is only to be expected when the spring's extension has decreased to 22 nm, with the motor in the S1 state. The time required for force relaxation from F_{start} (2.9 at an extension of 44 nm) to F_{jump} (1.0 pN at 22 nm) depends on the size of the cargo, and is approximately 2 s for $\beta = 10^{-4}$ kg s^{-1}, in accordance with the simulated value of 1.8 ± 0.3 s.

In the soft spring system C1 the 2.3 and 3.8 pN thresholds are irrelevant, because, with $\beta = 10^{-4}$ kg s^{-1}, the restoring force of the spring is always greater than 2.3 pN. The steady-state velocity depends only on the frequency of forward and backward stepping under load, and is calculated from the expression for the mean forward dwell time (Kolomeisky & Fisher 2003, see §2).

In system V1, on the other hand, the extension at which the restoring force F is 2.3 pN is 59 nm, and 65 nm for $F = 3.8$ nm. If the centre of force of the motor moves forward by 13.5 nm and the extension increases to 73 nm, the force increases far above 3.8 pN (to 15 pN), and in all likelihood the motor will rapidly make the backward transition S0←S1. In this case, the thresholds are crossed when the extension is 59 and 65 nm. Stepping now occurs in two phases, which are clearly visible in the close-up of the extension trajectory in figure 4. In the first phase, the spring extension decreases from 65 to 36, after which the motor can successfully make the 22.5 nm sub-step. In the second phase, the extension decreases from 59 to 51, from

where the next jump to 65 nm can be made. According to equation 2.6*b*, the times required for the spring to relax from 65 to 36 nm, and from 59 to 51 nm are 5.8 s and 0.7 s, respectively, in good agreement with the simulated period of 6.7 ± 0.3 s. As a result of the saw-tooth shape of the spring relaxation pattern in system V2, the difference between the longest and the shortest extension is only 29 nm (disregarding any aborted excursions to greater extensions): 80% of the 36 nm in C2 and V2.

4. GENERAL DISCUSSION

The dynamics of myosin-V dragging cargo on an elastic tether through a viscous medium were simulated by coupling a stochastic stepping model to a continuous damped spring description of cargo movement and associated force relaxation. In this model, the pulling force on the motor depends on the spring extension immediately after the last step, and decreases in the interval between two steps, owing to the movement of the cargo towards the motor. The correct simulation of this process requires storage of both the motor state and spring extension and re-evaluation of the reaction probability density function (Gillespie 1977) after each event. The theory of exact stochastic simulation of such non-Markov processes, based on Gillespie's direct method, has been previously outlined by Gibson & Bruck (2000), but to our knowledge this is the first example of a simulation in which a stochastic bio-chemical process elicits a continuous mechanical response, which then feeds back into the transition probabilities.

We have used a relatively simple two-state model of myosin-V processivity, which, as Kolomeisky & Fisher (2003) have shown, can quantitatively account for the observations on the force and nucleotide dependence of the dwell times by Rief *et al.* (2000), and has yielded parameter values that are in excellent agreement with estimates from previous studies. Many published models of myosin-V processivity include many more than two states (De La Cruz *et al.* 1999; Rief *et al.* 2000; De La Cruz *et al.* 2001; Mehta 2001; Baker *et al.* 2004; Lan & Sun 2005; Vilfan 2005), and almost certainly express certain (or all) aspects of its dynamics more precisely than the two-state model. However, the Kolomeisky & Fisher study provides a full, accessible complement of all parameter values (in particular those of the load distribution factors) that are required to set up a thermodynamically justifiable model that can be tested against published observations.

In this study, we have expressed the size and other hydrodynamic characteristics of the cargo as a single value: the frictional constant β. A rough estimate of the frictional constant of a spherical particle with radius R is obtained from Stokes' relation, $\beta = 6\pi R \eta$, where η is the viscosity of the (homogeneous and isotropic) medium (Atkins 1994). In an environment in which the viscosity is that of water at 20 °C (10^{-3} Pa s), a particle with a diameter of 1 cm (!) has a frictional constant of 10^{-4} kg s^{-1}, the 'standard' frictional constant used in this study. The cytosol has, of course, a much greater viscosity, but estimates strongly depend on the measurement technique, and vary from 3×10^{-3} to 10^3 Pa s (Freitas 1999). Measurement of the local viscoelasticity in macrophages using ferromagnetic beads of 1.3 μm diameter and optical tweezers yielded an effective viscosity of 210 ± 143 Pa s (Bausch *et al.* 1999). In such an environment, a spherical particle with a diameter of 1 μm has a frictional constant β of 2 (± 1)$\times 10^{-3}$ kg s^{-1} ($\equiv$ Pa m s), and a vesicle with $\beta = 10^{-4}$ kg s^{-1} would have a diameter of 50 nm. The cytosol, however, is neither homogeneous nor isotropic, and its effective viscosity is likely to be dependent on particle size.

In our simulations and calculations, we have neglected the effect of Brownian noise, although considerable fluctuations due to thermal effects are expected (of the order of 10 nm for $\kappa = 0.05$, and 30 nm for $\kappa = 0.005$ pN nm^{-1}). A quantitative analysis of the effects of thermal noise is beyond the scope of this study. However, we expect that, for springs whose stiffness increases with extension, thermal noise will shorten the spring relaxation times to some extent, as a collision of the cargo with a particle that is moving in the direction of the spring's restoring force will result in a greater change in extension than a collision with a particle travelling in the opposite direction.

We have compared the simulated behaviour of systems with two types of fully elastic springs: springs whose stiffness is independent of their extension, and springs whose stiffness increases when they stretch. Like all springs, the coiled-coil domain of myosin-V is almost certainly of the second kind, and if its characteristics are similar to those of the coiled-coil domain in myosin-II (Schwaiger *et al.* 2002), it will stretch relatively easily until its length has increased by a factor of 1.5. At higher extensions, its stiffness increases steeply, and stretching it further becomes much more difficult. We observe that the stepping efficiency and regularity depend strongly on the spring characteristics, and can distinguish three types of behaviour.

(i) Systems in which the spring is very soft at all extensions move forward along the track in an essentially random manner. If the load is small, only forward stepping is observed, but with larger loads, the number of backward sub-steps (mainly the 22.5 nm S0 ← S1 transition) increases, and the overall velocity of the system decreases as a result. In these systems, it is not unusual to observe several consecutive full reverse steps, even if the ratio fraction of reverse steps is small. Because the force on the motor is virtually constant in such (hypothetical) systems, their simulated behaviour is very similar to that observed *in vitro* in single molecule studies where the force on myosin-V is kept constant through an electronic feedback system.

(ii) Systems in which κ is constant, but so high that a forward step of 36 nm under load results in a significant increase in the spring's restoring force (κ of the order of 0.01 to 0.1 pN nm^{-1}), also move randomly when dragging small loads

($\beta < 1 \times 10^{-6}\,\mathrm{kg\,s^{-1}}$). At higher loads, stepping becomes more regular as the spread in the length of the intervals between two full forward steps decreases. For large loads the duration of the delay between steps is determined by the relaxation time of the spring – cargo combination. Motor, spring and cargo form a true escapement, as the motor is only allowed to 'escape' from its current position when the force has fallen below the system's lower threshold at 2.3 pN. Once the force on the motor has fallen below this threshold, and the motor is in the S0 state, it is more likely that the motor will make a forward sub-step than a backward one. Nonetheless, the motor makes occasional full backward steps, but only to compensate a previous forward step that occurred 'early'. However, in contrast to the soft spring systems it never makes two or more consecutive backward steps. As a result, the deviations of the motor from the path of uniform motion become smaller. A similar behaviour is exhibited by systems in which κ is dependent on the spring's extension, provided there is a region in their force – extension profile where the average slope over 36 nm is in the range of 0.01 to 0.1 pN nm^{-1} (such as figure 2, curve V2).

(iii) Systems in which the spring's force – extension curve increases very rapidly over a short distance (figure 2, curve V1) move even more regularly and uniformly under load than the systems discussed under (ii)). The trajectory of the spring's extension has a typical double sawtooth pattern, in which, during a single cycle, the extension gradually decreases, then rapidly increases, relatively slowly decreases again before it jumps up again, as illustrated in figure 5. This behaviour is caused by the presence of two thresholds ('escapes'), one at 2.3 (see above), and one at 3.8 pN. The upper threshold is situated at the point above which backward stepping from S0 is more likely than forward stepping. This threshold is only traversed in systems in which the 13.5 nm forward step increases the spring's restoring force by more than 1.5 ($=3.8-2.3$) pN. The overall variation in spring extension is smaller in these double-escape systems than in the single-escape ones (29 nm in V1 versus 36 nm in C2, disregarding aborted 13.5 nm excursions to greater extensions), and the oscillatory period is also more sharply defined. The spring in systems of this type must be sufficiently long and sufficiently soft at small extensions, as it needs to be able to extend by 22.5 nm without the force exceeding 2.3 pN. The spring is 'too short' when the value of b is larger than 0.047 pN$^{(0.1)}$ nm^{-1} (for $a=0.005$ and $p=10$), i.e. when it is shorter than about 27 nm (contour length). It is 'too stiff' at small extensions when a is larger than 0.1 (for $b=0.018$ and $p=10$), which corresponds to a persistence length of 1.3 nm. However, even under those conditions the motor will
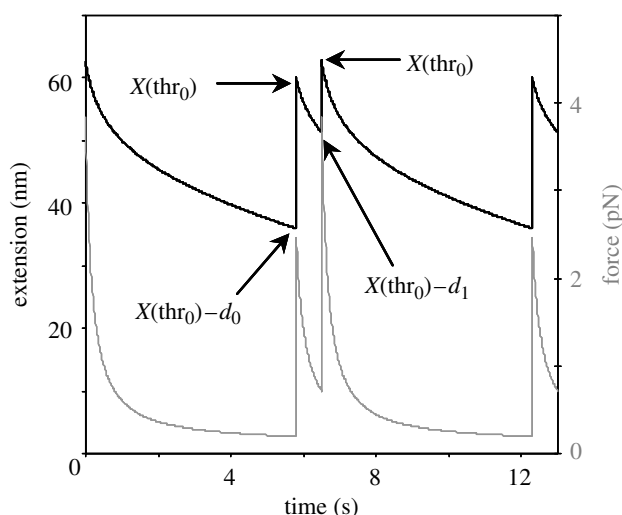

Figure 5. Typical 'saw-tooth' pattern of the spring extension and restoring force over two oscillatory periods for two-threshold systems (see text). Black line, left hand vertical axis: extension (equation (2.6b)); grey line, right-hand axis: force ($= ax + (bx)^P$); constructed with the parameters and thresholds for system V1 (see table 1). $X(\mathrm{thr}_0)$: and $X(\mathrm{thr}_1)$ extension at force thresholds 0 and 1(here 2.3 and 3.8 pN); d_0 and d_1: sub-step sizes (here 13.5 and 22.5 nm).

occasionally make a forward step, because it still has a finite probability to do so.

On the whole, an increase in regularity goes hand in hand with a decrease in velocity: while moving at 20 nm s^{-1}, system C1, which makes steps at random intervals, can drag a 30% larger cargo than C2, which moves in a much more regular manner. On the other hand, system V1, whose oscillatory period is best defined, needs its load reduced by 80% with respect to that of C1, to reach the same velocity. The average force on the motor is correspondingly smaller in the more regular systems.

Although the relevant characteristics of the coiled-coil domain in myosin-V still remain to be determined experimentally, the analogy with myosin-II suggests that myosin-V is a double-escape system. In general, the behaviour of a particular system can be understood from the position of the thresholds (of which there may be more than two in more complex models), the length of the sub-steps, and the spring extension at the thresholds.

Since we have used stochastic, rather than continuous equations to model the motor dynamics, during each cycle the motor's centre of force travels back and forth 22.5 and 13.5 nm with a high frequency. In reality it is more likely that both the S1→S0 and S0→S1 transitions are relaxation processes, triggered by instantaneous events that change the position of the thermodynamic equilibrium, such as ATP binding or Pi and ADP release. However, the model, which is entirely thermodynamic in nature, makes no further assumptions about chemical or mechanical cause and effect.

Thus, if the properties of the myosin-V coiled-coil region are similar to those of the corresponding myosin-II region, and if the drag of its natural cargo causes significant changes in the restoring force of the tether, it

is predicted that the motion of a myosin-V-vesicle combination *in vivo* is highly regular. This would, of course, have great advantages on a crowded actin filament, particularly where a large load is dragged by more than one myosin-V unit. Since the motion of the individual motors is uniform, they can move closely together without running into each other. Furthermore, as has already been argued convincingly for muscle contraction (which involves actin filaments and myosin-II bundles; Duke 1999): when multiple units pull a single, large load, their stepping will almost certainly become coordinated: one unit making a forward step alleviates the force on the other units. As a result, its own backward (S1←S0) stepping rate increases, and it will not make another full forward step for a while, and conversely, the other units become more likely to make a successful forward step. Therefore, we predict that the forward stepping of 'teamed-up' myosin-V units will tend to cluster around particular times, and stepping will synchronize.

REFERENCES

Atkins, P. W. 1994 *Physical chemistry*, 7th edn. Oxford, UK: Oxford University Press.

Baker, J. E., Krementsova, E. B., Kennedy, G. G., Armstrong, A., Trybus, K. M. & Warshaw, D. M. 2004 Myosin V processivity: multiple kinetic pathways for head-to-head coordination. *PNAS* **101**, 5542–5546. (doi:10.1073/pnas.0307247101)

Bausch, A. R., Möller, W. & Sackmann, E. 1999 Measurement of local viscoelasticity and forces in living cells by magnetic tweezers. *Biophys. J.* **76**, 573–579.

Bortz, A. B., Kalos, M. H. & Lebowitz, J. L. 1975 A new algorithm for Monte Carlo simulation of Ising spin systems. *J. Comput. Phys.* **17**, 10–18. (doi:10.1016/0021-9991(75)90060-1)

Bustamante, C., Marko, J. F., Siggia, E. D. & Smith, S. 1994 Entropic elasticity of lambda-phage DNA. *Science* **265**, 1599–1600.

Clemen, A. E. M., Vilfan, M., Jaud, J., Zhang, J., Barmann, M. & Rief, M. 2005 Force-dependent stepping kinetics of myosin-V. *Biophys. J.* **88**, 4402–4410. (doi:10.1529/biophysj.104.053504)

De La Cruz, E. M., Wells, A. L., Rosenfeld, S. S., Ostap, E. M. & Sweeney, H. L. 1999 The kinetic mechanism of myosin V. *PNAS* **96**, 13 726–13 731. (doi:10.1073/pnas.96.24.13726)

De La Cruz, E. M., Ostap, E. M. & Sweeney, H. L. 2001 Kinetic mechanism and regulation of myosin VI. *J. Biol. Chem.* **276**, 32 373–32 381. (doi:10.1074/jbc.M104136200)

Duke, T. A. J. 1999 Molecular model of muscle contraction. *Proc. Natl Acad. Sci. USA* **96**, 2770–2775. (doi:10.1073/pnas.96.6.2770)

Espreafico, E. M., Cheney, R. E., Matteoli, M., Nascimento, A. A., De Camilli, P. V., Larson, R. E. & Mooseker, M. S. 1992 Primary structure and cellular localization of chicken brain myosin-V (p190), an unconventional myosin with calmodulin light chains. *J. Cell Biol.* **119**, 1541–1557. (doi:10.1083/jcb.119.6.1541)

Evans, L., Lee, A., Bridgman, P. & Mooseker, M. 1998 Vesicle-associated brain myosin-V can be activated to catalyze actin-based transport. *J. Cell Sci.* **111**, 2055–2066.

Freitas, R. A. 1999 *Nanomedicine. Basic capabilities*, vol. I, 1st edn. Austin, TX: Landes Bioscience.

Gibson, M. A. & Bruck, J. 2000 Efficient exact stochastic simulation of chemical systems with many species and many channels. *J. Phys. Chem. A* **104**, 1876–1889. (doi:10.1021/jp993732q)

Gillespie, D. T. 1977 Exact stochastic simulation of coupled chemical reactions. *J. Phys. Chem.* **81**, 2340–2361. (doi:10.1021/j100540a008)

Happel, J. & Brenner, H. 1983 *Low Reynolds number hydrodynamics with special applications to particulate media*, pp. 40–49. Dordrecht: Kluwer Press.

Kolomeisky, A. B. & Fisher, M. E. 2003 A simple kinetic model describes the processivity of myosin-V. *Biophys. J.* **84**, 1642–1650.

Lan, G. & Sun, S. X. 2005 Dynamics of myosin-V processivity. *Biophys. J.* **88**, 999–1008. (doi:10.1529/biophysj.104.047662)

Maita, T., Yajima, E., Nagata, S., Miyanishi, T., Nakayama, S. & Matsuda, G. 1991 The primary structure of skeletal muscle myosin heavy chain: IV. Sequence of the rod, and the complete 1,938-residue sequence of the heavy chain. *J. Biochem. (Tokyo)* **110**, 75–87.

Mehta, A. 2001 Myosin learns to walk. *J. Cell Sci.* **114**, 1981–1998.

Mehta, A. D., Rock, R. S., Rief, M., Spudich, J. A., Mooseker, M. S. & Cheney, R. E. 1999 Myosin-V is a processive actin-based motor. *Nature* **400**, 590–593. (doi:10.1038/23072)

Press, W. H., Flannery, B. P., Teukolsky, B. P. & Vetterling, W. T. 1989 *Numerical recipes. The art of scientific computing Fortran version*. Cambridge, UK: Cambridge University Press.

Reck-Peterson, S. L., Provance Jr, D. W., Mooseker, M. S. & Mercer, J. A. 2000 Class V myosins. *Biochim. Biophys. Acta (BBA)—Mol. Cell Res.* **1496**, 36–51. (doi:10.1016/S0167-4889(00)00007-0)

Rief, M., Fernandez, J. M. & Gaub, H. E. 1998 Elastically coupled two-level systems as a model for biopolymer extensibility. *Phys. Rev. Lett.* **81**, 4764–4767. (doi:10.1103/PhysRevLett.81.4764)

Rief, M., Rock, R. S., Mehta, A. D., Mooseker, M. S., Cheney, R. E. & Spudich, J. A. 2000 Myosin-V stepping kinetics: a molecular model for processivity. *PNAS* **97**, 9482–9486. (doi:10.1073/pnas.97.17.9482)

Schwaiger, I., Sattler, C., Hostetter, D. R. & Rief, M. 2002 The myosin coiled-coil is a truly elastic protein structure. *Nat. Mat.* **1**, 232–235. (doi:10.1038/nmat776)

Sellers, J. R. 2000 Myosins: a diverse superfamily. *Biochim. Biophys. Acta (BBA)—Mol. Cell Res.* **1496**, 3–22. (doi:10.1016/S0167-4889(00)00005-7)

Tabb, J., Molyneaux, B., Cohen, D., Kuznetsov, S. & Langford, G. 1998 Transport of ER vesicles on actin filaments in neurons by myosin V. *J. Cell Sci.* **111**, 3221–3234.

Titus, M. A. 1997 Motor proteins: myosin V—the multipurpose transport motor. *Curr. Biol.* **7**, R301–R304. (doi:10.1016/S0960-9822(06)00143-6)

Trybus, K. M., Krementsova, E. & Freyzon, Y. 1999 Kinetic characterization of a monomeric unconventional myosin V construct. *J. Biol. Chem.* **274**, 27 448–27 456. (doi:10.1074/jbc.274.39.27448)

Uemura, S., Higuchi, H., Olivares, A. O., De La Cruz, E. M. & Ishiwata, S. 2004 Mechanochemical coupling of two substeps in a single myosin V motor. *Nat. Struct. Mol. Biol.* **11**, 877–883. (doi:10.1038/nsmb806)

Vale, R. D. 2003 Myosin V motor proteins: marching stepwise towards a mechanism. *J. Cell Biol.* **163**, 445–450. (doi:10.1083/jcb.200308093)

Veigel, C., Wang, F., Bartoo, M. L., Sellers, J. R. & Molloy, J. E. 2001 The gated gait of the processive molecular motor, myosin V. *Nat. Cell Biol.* **4**, 59–65. (doi:10.1038/ncb732)

Veigel, C., Schmitz, S., Wang, F. & Sellers, J. R. 2005 Load-dependent kinetics of myosin-V can explain its high processivity. *Nat. Cell Biol.* **7**, 861–869. (doi:10.1038/ncb1287)

Vilfan, A. 2005 Elastic lever-arm model for myosin V. *Biophys. J.* **88**, 3792–3805. (doi:10.1529/biophysj.104.046763)